CENTRE DE RECHERCHE EN TECHNOLOGIE DES PLASMAS (CRTP)

PLASMA TECHNOLOGY RESEARCH CENTRE

**FINAL REPORT**

# PLASMA SYNTHESIS OF ULTRAFINE SILICON CARBIDE POWDERS
# SYNTHESE DES POUDRES ULTRAFINES DE CARBURE DE SILICIUM PAR PLASMA

By:

**C. Laflamme, J. Jurewicz and M.I. Boulos**
CRTP, Department of Chemical Engineering
Université de Sherbrooke
Sherbrooke, Qué, Canada, J1K 2R1
Tel: (819) 821-7168
FAX: (819) 821-7955

Submitted to:

**Dr. S. A. Mikhail**
**Dr. J. M. Skeaf**
Energy Mines and Resources
Mineral Sciences Division
555 Booth Street
Ottawa, Ontario, K1A OG1
Tel: (613) 992-4328
FAX: (613) 996-9673

**Conducted under the terms of contract agreement 23440-7-9180/01-SS**
**for the period October 1st 1987 to September 30th 1989**

41 pp

**Sherbrooke, April 30 1990**

MICROMEDIA

## EXECUTIVE SUMMARY

A feasibility study is carried out for the plasma synthesis of ultrafine powders of silicon carbide. The proposed approach is based on the direct carburization of silicon vapor/condensed droplets using methane as quench gas. The chemical transformation involved is:

$$Si + CH_4 \rightarrow SiC + 2H_2$$

The work presented in this report involved both a theoretical and an experimental study. Their scopes and the principal results obtained can be summarized as follows.

**a) Theoretical analysis**

This involved, in the first place, calculations of the equilibrium composition for different initial reaction mixtures ($1.0 < C/Si < 1.25$) over a wide range of temperatures ($300 < T < 6000$ K) and pressures ($0.5 < P < 2.0 \times 10^5$ Pascal). The results show that the formation of SiC is generally favored at temperatures below 2900 K. The effect on the equilibrium composition of the presence of $N_2$, as the plasma gas, and $H_2O$, as humidity in the reactants, is also investigated.

The theoretical study also involved the development of a kinetic model which served to estimate the reaction time required for complete conversion. The results showed the rapid formation of b-SiC in a few milliseconds though equilibrium composition was attained only after 200 to 300 ms.

**b) Experimental study**

Different reactor designs were tested based on the use of separate sections for the plasma vaporization of elemental silicon, and the quench and carburization of the silicon vapors using methane. The formed silicon carbide powder was collected in a venturie scrubber using a light hydrocarbon as scrubbing fluid. Conversions of 90-98% were obtained with close to 50% product recovery. The collected powder had a b-SiC/Total SiC ratio of 70 to 90%. The free carbon content could be reduced to 1 to 4% with the free silicon less than 1%. The mean specific surface area of the powder was of the order of 30 to 60 $m^2/g$ with a corresponding mean particle diameter in the range of 60 to 30 nm. The results of the experimental study also revealed a strong dependence of the free carbon and of the free silicon content of the powder on the operating pressure and the methane gas flow rate.

**PLASMA SYNTHESIS OF ULTRAFINE SILICON CARBIDE POWDERS**
**SYNTHESE DES POUDRES ULTRAFINES DE CARBURE DE SILICIUM PAR PLASMA**

## 1. INTRODUCTION

The plasma synthesis of ultrafine powders (UFP) of ceramics such as SiC and $Si_3N_4$ has been the subject of numerous studies. The principal advantages of the plasma technology route over alternative approaches has generally been recognized in its ability to maintain a high level of purity of the product and a close control on the particle size which is typically below 0.1 μm. It also offers the possibility of particle doping on a microscale during the synthesis step which facilitate the subsequent sintering of the powder to near theoretical density bodies with superior mechanical and thermal properties. The plasma route, however, suffers from being a relatively new technology with no large scale industrial plants in operation in the advanced ceramic area. The production cost also tend to be relatively high because of the use of expensive raw materials or high energy demands.

Realizing the important potential of plasma technology in this area, the objective of the present investigation is to carry out a feasibility study for the plasma synthesis of high purity ultrafine powders of silicon carbide. A special attention is given to raw material and energy cost in the selection of the reaction route and the reactor design used. Priority has been given to the possible use of relatively low-cost raw materials such as silica or elemental silicon as starting material in favor over more expensive traditional feedstocks such as silane or silicon tetrachloride used by earlier investigations in this field. The reactor design used has also been developed with the principal concern of energy efficiency in view of minimizing the specific energy requirement of the process. Because of scale effects, no attempt has been made at this stage of the investigation, to extract from the results presented in this report meaningful specific energy requirement data for the proposed process.

## 2. THEORETICAL CONSIDERATIONS

A wide range of reaction routes have been proposed in literature for the plasma synthesis of silicon carbide powders. These include,

$$Si + C \longrightarrow SiC \quad (1)$$

$$SiO_2 + 3C \longrightarrow SiC + 2CO \quad (2)$$

$$SiO(g) + CH_4 \longrightarrow SiC + H_2O + H_2 \quad (3)$$

$$SiO + 3CO \xrightarrow{<800°C} SiC + 2CO_2 \quad (4)$$

$$3SiO + CO \xrightarrow{<1650°C} SiC + 2SiO_2 \quad (5)$$

$$SiH_4 + CH_4 \longrightarrow SiC + 4H_2 \quad (6)$$

$$SiCl_4 + CH_4 \longrightarrow SiC + 4HCl \quad (7)$$

$$CH_3SiCl_3 \longrightarrow SiC + 3HCl \quad (8)$$

$$(2CH_3\text{-}Si)_n \xrightarrow{<600°C} nSiC + nC + 3nH_2 \quad (9)$$

In spite of its simplicity, the direct carburization of elemental silicon using methane, according to the following equation, does not seem to have attracted much attention.

$$Si + CH_4 \longrightarrow SiC + 2H_2 \quad (10)$$

It offers, however, a number of important advantage which made us focus on it in the present investigation. These include the relatively low cost of the starting materials, Si and $CH_4$, and the absence of any chlorides in the system liable to contaminate the product with HCl and/or free chlorine. The reaction allows for control of the particle size through proper adjustment of the quench rate. It also offers the possibility of in-situ doping of the powder on a microscale through the proper adjustment of the chemical composition of the reaction mixture.

In order to establish a good theoretical basis for our work on this last reaction using the plasma route, a series of thermodynamic equilibrium calculations and a kinetic study were carried out in the first stages of this investigation.

## 2.1 Equilibrium calculations

The thermodynamic equilibrium calculations for the [Si-C-H] system were carried out using a standard Gibbs free energy minimization scheme over the temperature range of 300-6000 K. The following species are considered for the computations.

| | | |
|---|---|---|
| C(s) | $C_3$ | SiH+ |
| C | $C_3H$ | $SiH_2$ |
| C- | $C_4H$ | $SiH_3$ |
| C+ | $C_4H_2$ | $SiH_4$ |
| CH | $C_4H_4$ | $Si_2$ |
| CH+ | H | $Si_3$ |
| $CH_2$ | H+ | $Si_2H_2$ |
| $CH_3$ | H- | A-SiC(s) |
| $CH_4$ | $H_2$ | B-SiC(s) |
| $C_2$ | $H_2$+ | SiC |
| $C_2$- | Si(s) | $Si_2C$ |
| $C_2H$ | Si(1) | $SiC_2$ |
| $C_2H_2$ | Si | e- |
| $C_2H_4$ | Si+ | |
| $C_2H_6$ | SiH | |

Values of the Gibbs free energies for the different species were mostly taken from the JANAF tables and other literature data. In order to reduce the computational time, not all the species were simultaneously taken into account over the full temperature range. Based on preliminary calculations, the number of species considered could be limited as follows for each of the indicated temperature range.

**300 < T < 1600 K**

| | | |
|---|---|---|
| C(s) | $C_4H_2$ | SiH |
| $CH_3$ | $C_4H_4$ | $SiH_2$ |
| $CH_4$ | H | $SiH_4$ |
| $C_2H$ | $H_2$ | b-SiC(s) |
| $C_2H_2$ | Si(s) | |
| $C_2H_4$ | Si(1) | |
| $C_2H_6$ | Si | |

**1600 < T < 4000 K**

| | | |
|---|---|---|
| C(s) | $C_3$ | Si+ |
| C | $C_3H$ | SiH |
| C- | $C_4H$ | $SiH_2$ |
| CH | $C_4H_2$ | $Si_2$ |
| $CH_2$ | H | $Si_2H_2$ |
| $CH_3$ | H+ | $Si_3$ |
| $CH_4$ | $H_2$ | b-SiC(s) |
| $C_2$ | Si(s) | SiC |
| $C_2H$ | Si(1) | $SiC_2$ |
| $C_2H_2$ | Si | $Si_2C$ |

**4000 < T < 6000 K**

| | | |
|---|---|---|
| C | $C_3$ | Si+ |
| C+ | $C_3H$ | SiH |
| C- | $C_4H$ | SiH+ |
| CH | H | $SiC_2$ |
| CH+ | H+ | SiC |
| $C_2$ | H- | $Si_2$ |
| $C_2$- | $H_2$ | $Si_3$ |
| $C_2H$ | $H_2$+ | e- |
| $C_2H_2$ | Si | |

It may be noted that only the cubic form of (b-SiC) is included since a-SiC is slightly less stable than b-SiC (by about 1.7 kJ/mole) and accordingly does not appear in the equilibrium diagrams. $SiH_3$ is also not included in this list since its free energy is comparable with $SiH_2$ and $SiH_4$, both of which, whenever present in the equilibrium mixture, appeared at very low concentrations.

Computations were carried out for different stoechiometric ratios of $CH_4/Si$ = 0.5, 1.0, 1.25 and 2.0 at atmospheric pressure, and for the $CH_4/Si$ = 1.0 case at pressures of 0.5 and 2.0 atm. Attention was also given to the effect of the presence of nitrogen in the system as the plasma gas ($N_2/Si$ = 10), and to the effect of small quantities of humidity ($H_2O/Si$ = 0.1), on the equilibrium composition.

Typical results, given in Figures 1-5, show the equilibrium composition for different mixtures at atmospheric pressure over the temperature range 300-4000 K. While earlier computations were extended to 6000 K, the results between 4000 and 6000 K were of little interest since the gas composition in this temperature range is dominated by monoatomic species such as Si, C, H, which represent close to 95% (molar) of the species present. Variations of the operating pressure over the range 0.5-2.0 atm also had only a marginal influence on the equilibrium composition and resulted simply in the shifting of the equilibrium curves on the temperature scale. For practical reasons operation at atmospheric pressure is adopted for the present study.

Figure 1 shows that silicon carbide is a very stable compound below its vaporization temperature of 2900 K. In a stoechiometric mixture of $CH_4/Si$, SiC is the only species present between 800-2900 K. Above that temperature SiC decomposes into a wide range of atomic and molecular species including Si, C, H and unstable radicals. In the presence of excess carbon ($CH_4/Si = 1.25$), the equilibrium curves has similar characteristics except for the presence of free carbon and $H_2$ below 2900 K. (Figure 2).

In the presence of nitrogen as plasma gas ,$N_2/Si = 10$, the equilibrium composition is considerably more complex with both SiC and $Si_3N_4$ appearing in the mixture. (Figure 3). Between 1650 and 2900 K, $N_2$ and b-SiC dominate the system with $Si_3N_4$ less than 0.3% w, while, below 1650 K, the situation is reversed with the dominant species being $N_2$, $Si_3N_4$ and free C with no SiC present. Because of the relatively low reaction rates at temperatures below 1650 K, the formation of $Si_3N_4$ can be avoided through the rapid quench of the product from 2000-3000 K down to room temperature.

The results given in Figures 4 and 5, deals with the effect of the presence of oxygen in the system as $H_2O$ in small initial concentrations ($H_2O/Si = 0.1$ molar) for a stoechiometric mixture ($CH_4/Si = 1.0$), and in the presence of excess carbon ($CH_4/Si = 1.25$) respectively. The results still show a predominance of b-SiC below 2900 K. A number of oxides of carbon and Si are present, however, in this temperature range causing a slight reduction in the SiC equilibrium concentration. The use of excess $CH_4$, ($CH_4/Si = 1.25$) reduces significantly the silicon carbide oxidation by fixing most of the oxygen as CO.

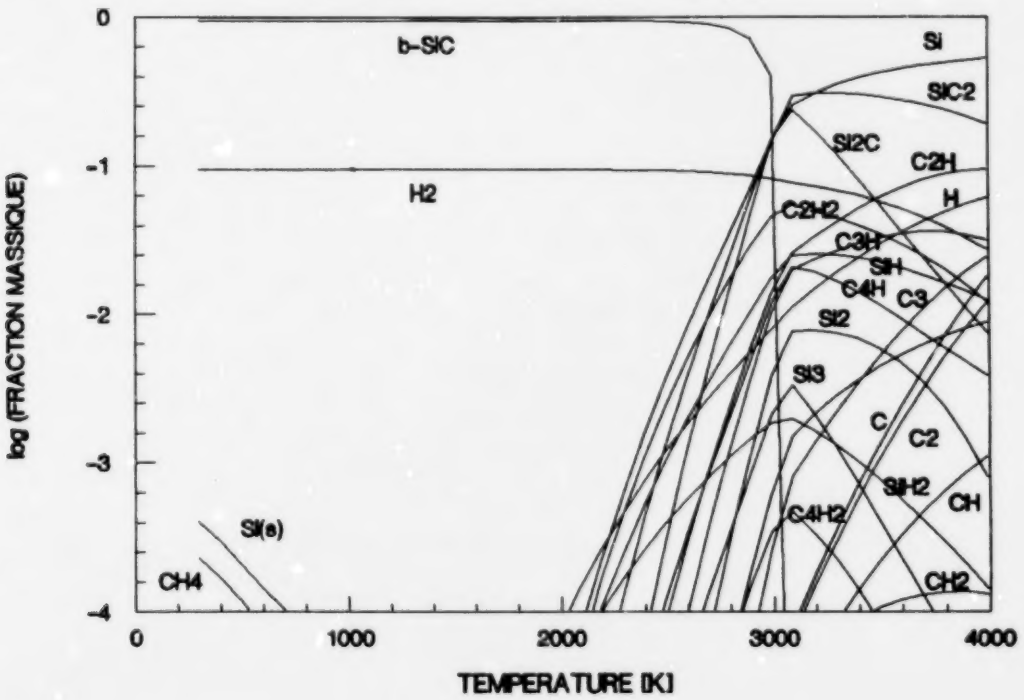


**Figure 1: Equilibrium composition at atmospheric pressure for a stoechiometric mixture $CH_4/Si = 1.0$**

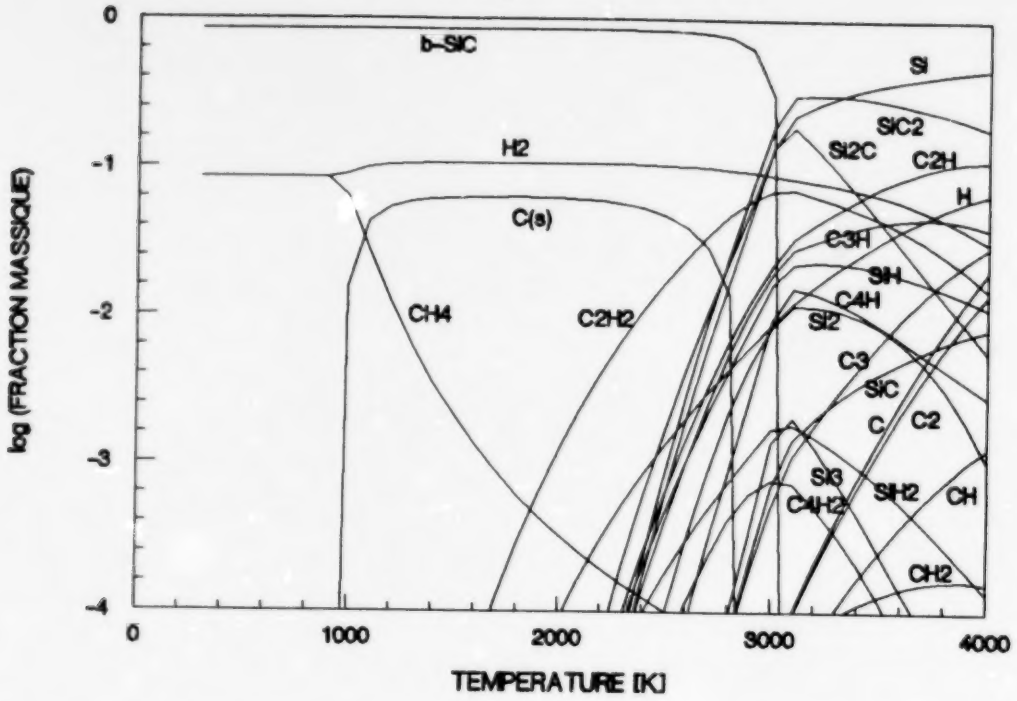


**Figure 2: Equilibrium deposition at atmospheric pressure in the presence of excess carbon $CH_4/Si = 1.25$**

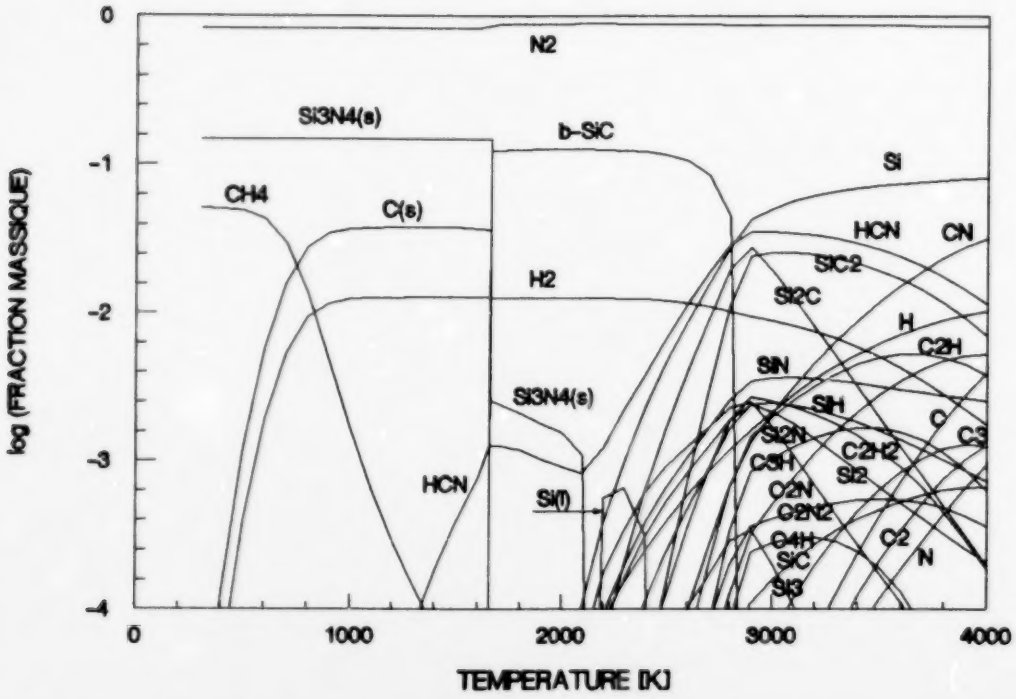


**Figure 3: Effect of the presence of nitrogen on the equilibrium composition at atmospheric pressure $CH_4/Si = 1.0$, $N_2/Si = 10$**

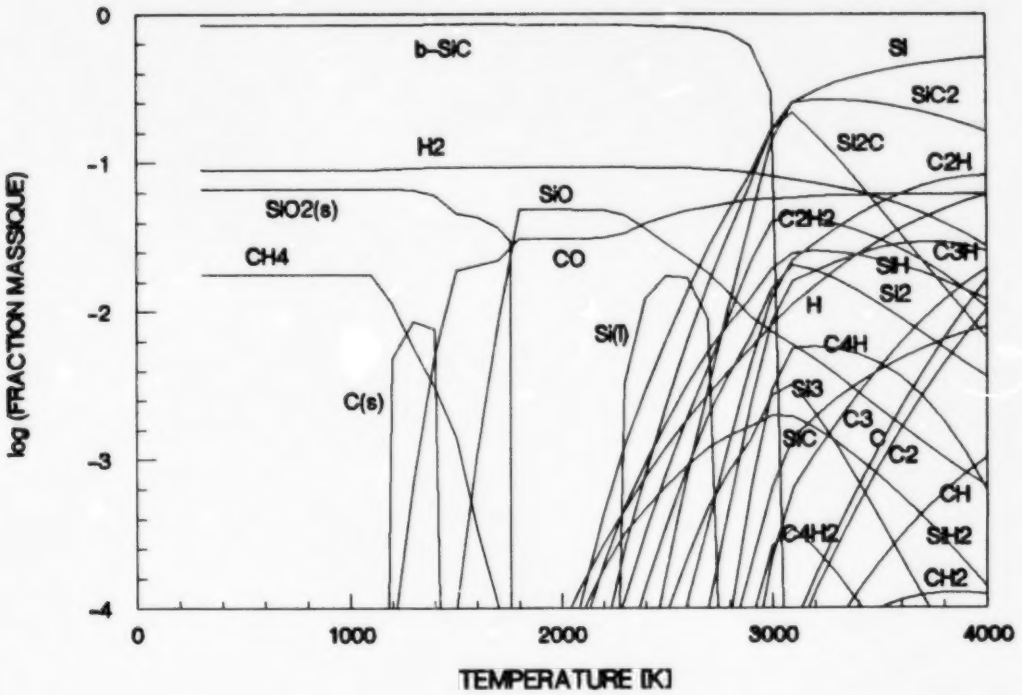


**Figure 4: Effect of the presence of water vapor on the equilibrium composition at atmospheric pressure $CH_4/Si = 1.0$. $H_2O/Si = 0.1$**

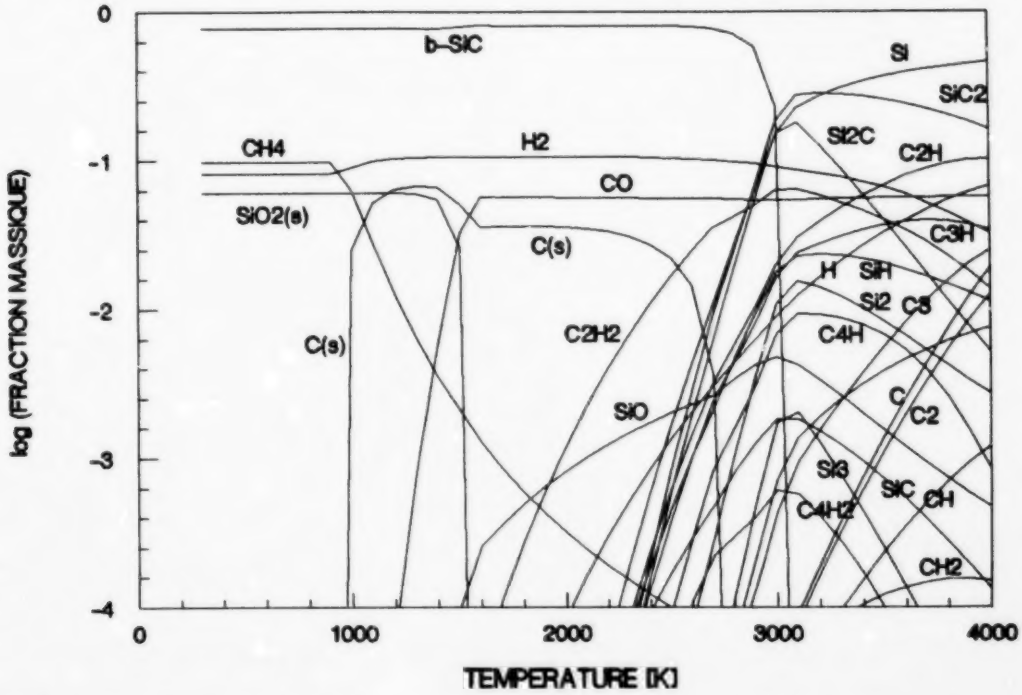


**Figure 5: Effect of the presence of water vapor on the equilibrium composition at atmospheric pressure $CH_4/Si = 1.25$, $H_2O/Si = 0.1$**

## 2.2 Kinetic model

A detailed kinetic model was developed in order to obtain an estimate of the required reaction time to approach the equilibrium concentrations. The model includes 324 elementary reactions and involves 30 chemical species. This was based on the following bi-molecular reaction model

$$AB + C \rightarrow A + BC$$

The model implied the assumption that the reaction goes through the destruction and the formation of simple links. The specific reaction rate constants were calculated according to the following equations:

$$k = \left(\frac{k_B T}{h}\right)\left(\frac{RT}{P}\right)\exp\left[-0.95\,\frac{\Delta G}{RT} - 13 - \frac{1200}{T}\right] \quad \text{for} \quad \frac{\Delta G}{RT} > 0$$

and

$$k = \left(\frac{k_B T}{h}\right)\left(\frac{RT}{P}\right)\exp\left[-0.05\,\frac{\Delta G}{RT} - 13 - \frac{1200}{T}\right] \quad \text{for} \quad \frac{\Delta G}{RT} < 0$$

where
- $k$ = reaction rate constant
- $k_B$ = Boltzman constant
- $h$ = Planks constant
- $T$ = Absolute temperature (K)
- $P$ = Reference pressure = 1.0 atm
- $R$ = Ideal gas constant
- $\Delta G$ = Free energy change

For a unimolecular reaction of the type

$$ABC \rightarrow A + BC$$

the corresponding reaction rate constants were calculated as follows:

$$k = \left(\frac{k_B T}{h}\right)\exp\left[-0.95\,\frac{\Delta G}{RT} - 13 - \frac{1200}{T}\right] \quad \text{for the direct reaction}$$

and

$$k = \left(\frac{k_B T}{h}\right) \exp\left[-0.05\,\frac{\Delta G}{RT} - 13 - \frac{1200}{T}\right] \quad \text{for the reverse reaction}$$

Typical results obtained for an atmospheric pressure argon plasma at 2500 K with an initial stoechiometric mixture ($CH_4/Si = 1.0$), and in the presence of excess carbon ($CH_4/Si = 1.25$) are given in Figures 6 and 7 respectively. In these two cases, the ratio $Ar/Si = 5.0$ molar.

The results are given as the weight fraction of the different constituents of the reaction mixture are function of time. These show that the silicon will be mostly in the liquid phase at this temperature (T = 2500 K), and that the reaction between the $CH_4$ and Si will be completed in less than 0.3 s. The presence of excess carbon, $CH_4/Si = 1.25$, affects mostly the equilibrium composition rather than the reaction rate.

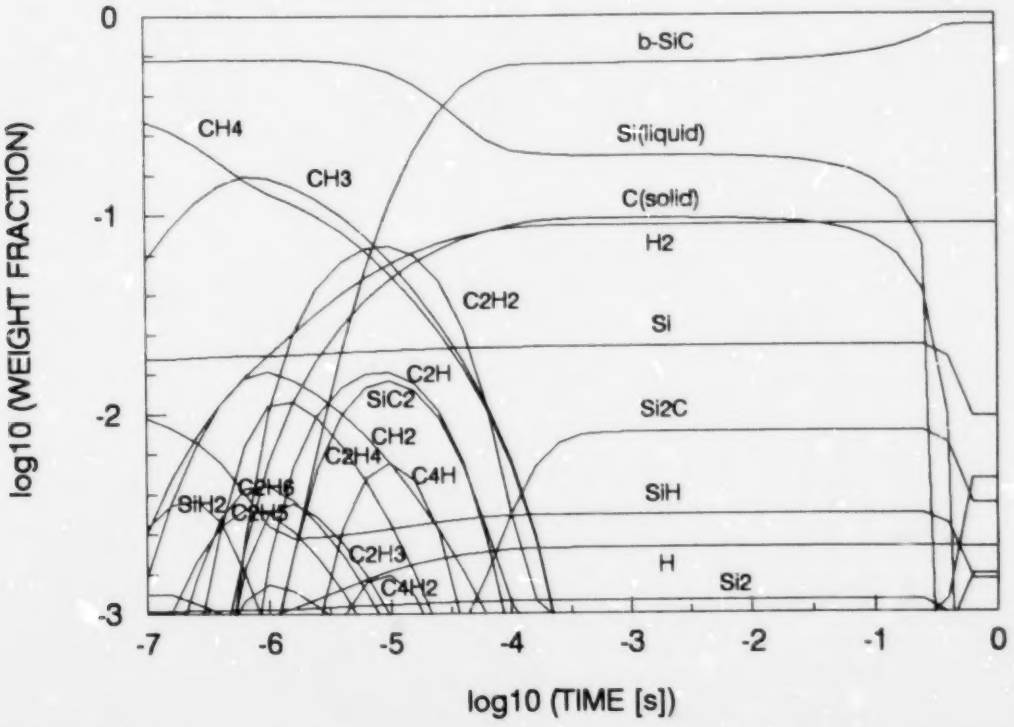


**Figure 6: Composition of the reaction mixture as a function of time for an argon plasma at atmospheric pressure and 2500 K, $Ar/Si = 5.0$, $CH_4/Si = 1.0$**

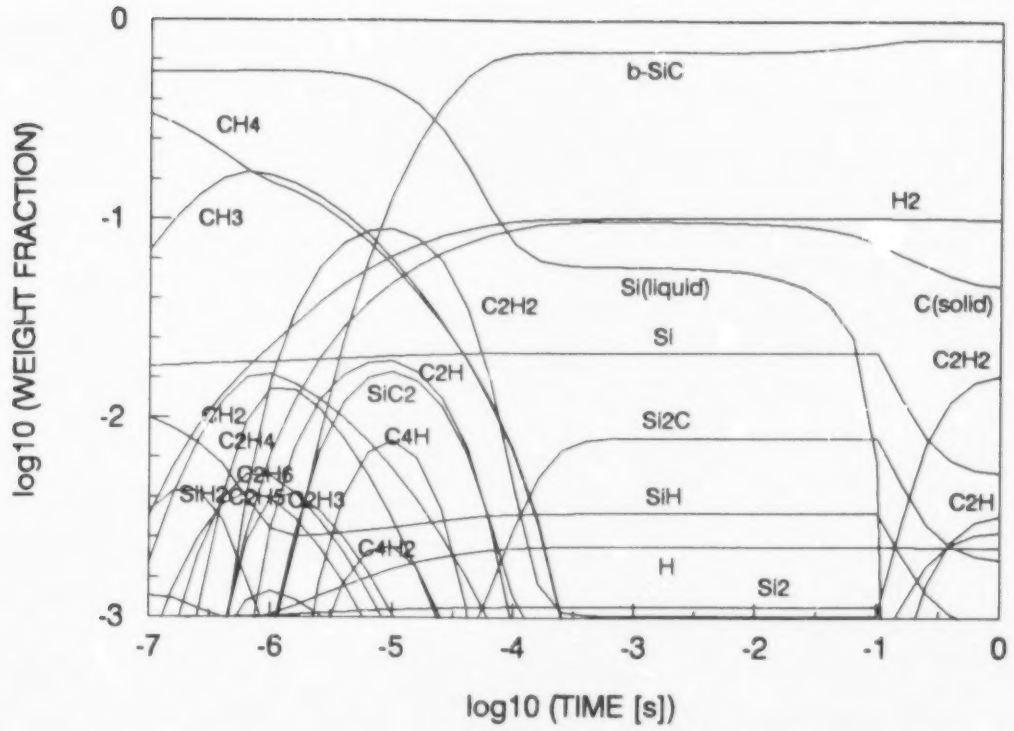


**Figure 7: Composition of the reaction mixture as a function of time for an argon plasma at atmospheric pressure and 2500 K, Ar/Si = 5.0, $CH_4$/Si = 1.25**

## 3. EXPERIMENTAL SET UP

The approach used in the present investigation involved essentially the vaporization of elemental silicon in a plasma reactor using a d.c. plasma torch followed by the condensation of the vapor of a fine aerosol of liquid silicon droplets which reacts rapidly with methane, used as the quench gas, to form an ultrafine powder of silicon carbide. Final cooling of the reaction products and collection of the formed powder was achieved in a venturie scrubber using an inert liquid hydrocarbon as a scrubbing fluid. This had the main advantage of achieving a continuous and efficient collection of the powder while keeping it at all times protected from contamination due to exposure to the air.

A schematic of the experimental set up used is given in Figure 8. This consists of the following principal sections.

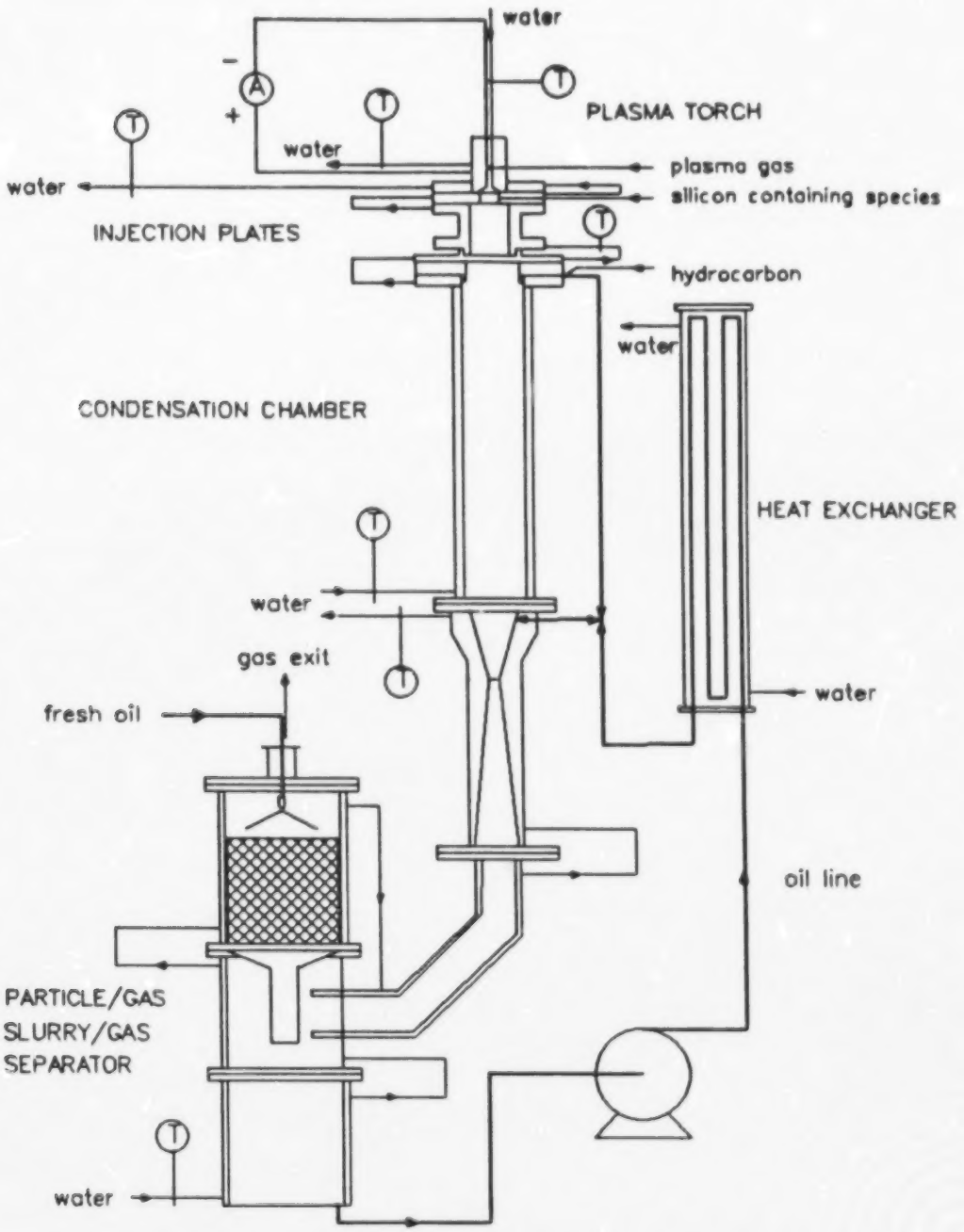


**Figure 8: Schematic of the experimental set up**

### 3.1 Plasma torch

The d.c. plasma torch used was of standard design with a thoriated tungsten cathode and a water-cooled copper anode, 5.0 mm i.d. It operated with either pure Ar, Ar/$H_2$ mixture or pure $N_2$ as the plasma gas with a gas flow rate in the range of 20-40 slpm. The arc current was a few hundred amps and the corresponding d.c. power 10-30 kW.

### 3.2 Silicon vaporization chamber

At the exit of the torch the plasma gas entered the silicon vaporization chamber. A number of designs illustrated schematically in Figures 9 and 10 were tested for this section. In the arrangement shown in Figure 9, the vaporization chamber is constructed of a water-cooled stainless steel cylindrical section, 55 mm i.d. by 65 mm long. In one configuration (Figure 9-a) the silicon powder was injected radially into the plasma jet through a 1.5 mm i.d. side orifice using argon as the powder carrier gas. As the silicon particles penetrated the plasma, it is rapidly heated, melted and partially vaporized in a relatively short time (<1 ms). This approach, however, had a relatively poor energy efficiency and gave rise to a number of operation problem due to the deposition of the unvaporized silicon on the walls of the chamber which eventually lead to its blockage. Part of the elemental silicon also found its way into the product as relatively large silicon granules which was detrimental to the product quality.

The dilute phase, powder vaporization, approach was later replaced by the silicon sleeve reactor design shown in Figure 9-b. In this case, the powder silicon was preformed in the shape of a cylindrical sleeve 9 mm i.d., 50 mm o.d. and 60 mm long which was placed in the reaction chamber concentric with the axis of the plasma jet. A small concentration of an organic binder (sucrose) is used to give the sleeve the necessary mechanical integrity for ease of handling without the need to go through any elaborate sintering steps. The plasma jet passed through the central channel of the sleeve heating its surface, melting and vaporizing it, in a relatively short time (a few minutes). This approach was most effective from an energy efficiency

point of view, since conduction, convection and radiation losses from the plasma jet were all received by the sleeve material and contributed to the heating, melting and vaporization steps.

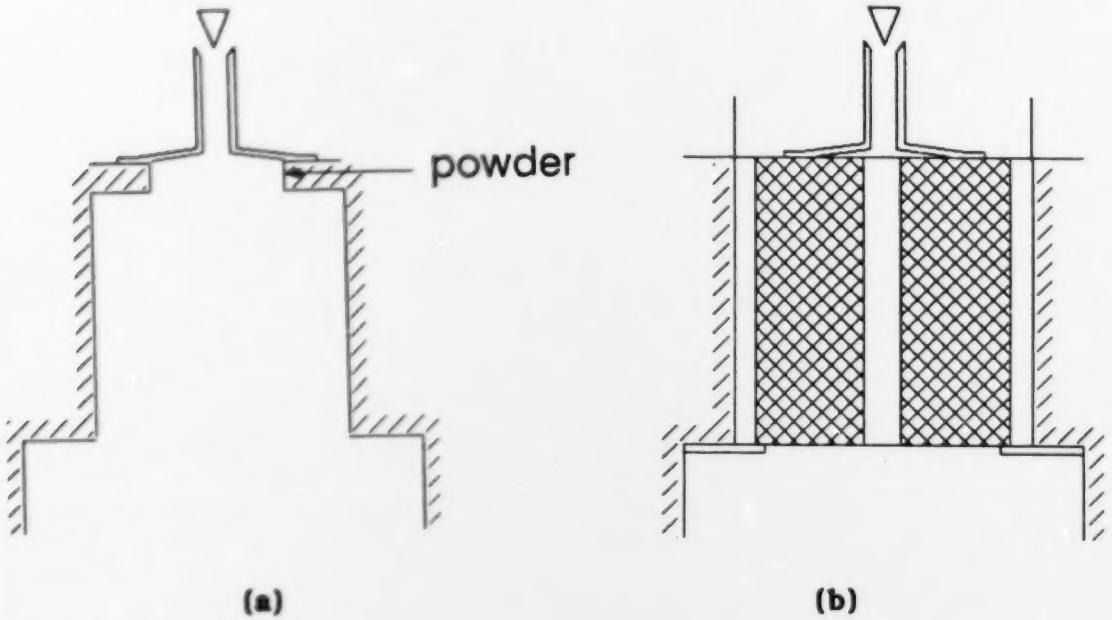


**Figure 9: Schematic of the designs used for the silicon vaporization chamber, (a) in-flight powder injection; (b) silicon sleeve vaporizer**

While relatively high vaporization rates, of the order of a few grams per minute, could be achieved using this approach the fact that the operation is batch with the silicon vaporization conditions changing in the course of an experiment, led us to explore alternative designs using the powder feeding technique. The reactor cavity was modified as shown in Figure 10 in order to collect the powder in a graphite crucible which could be directly heated by the plasma jet. The silicon powder was injected into the chamber using $Ar/CH_4$ mixture as the powder carrier gas.

This arrangement had substantially superior performance compared to the first powder feeding arrangement (Figure 9-a). It was not either completely immune from the problem of entrainment of some of the unvaporized silicon droplets/or particles with the gases which found its way into the product.

Certain problems were also caused by the condensation of the silicon vapor on the plasma torch and the tip of the powder feeding probe which in the latter case occasionally caused its blockage.

While further work is still needed to overcome some of the problem encountered in each of these three configurations of the silicon vaporization chamber, the sleeve approach seem to be the most favored for any long term developed because of its inherent high energy efficiency characteristics the high silicon vaporization rates that could be achieved in this case.

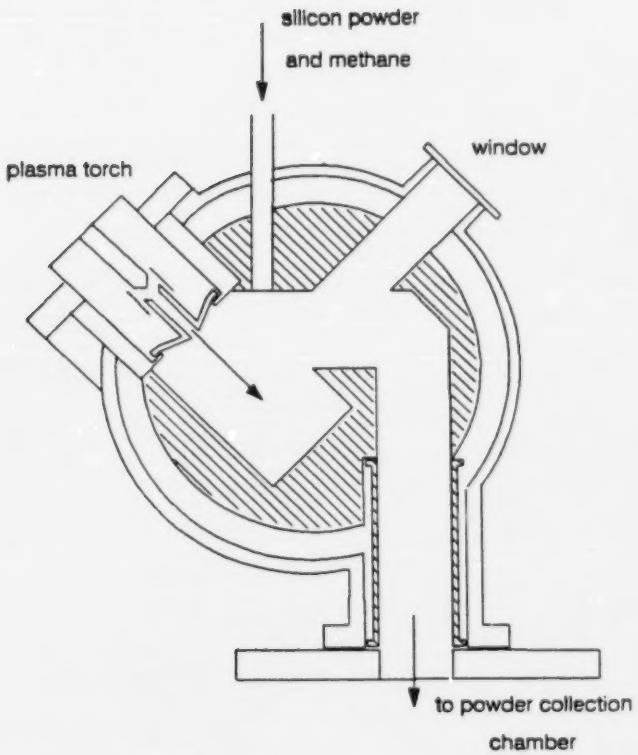


**Figure 10: The graphite crucible reactor design**

### 3.3 Condensation and powder collection sections

The silicon vapor mixed with the plasma gas was carburized through the injection of methane in the gas stream at the exit of the vaporization section. The gases/aerosols mixture passed through the condensation section formed of a water-cooled stainless steel cylinder 95 mm i.d., 550 mm long, followed by a venturie scrubber for final gas quench and collection of the product. At the exit of the venturie scrubber the gas/liquid mixture was separated in a cyclonic chamber and a demister to avoid the entrainment of any liquid droplets with the exhaust gases. The scrubbing fluid with its content of silicon carbide powder was collected in the bottom of this chamber and circulated in a closed loop using a diaphragm pump followed by a heat exchanger to avoid excessive hydrocarbon losses at the exit of the system. The formed silicon carbide powder was recovered at the end of the experiment as a slurry in the bottom of the collection chamber from which it was withdrawn, separated using a centrifuge, followed by vacuum drying.

Because of the critical role of the scrubbing fluid, special attention was given to the selection of the hydrocarbon to be used which had to have a relatively low viscosity for ease of circulation, while having a low vapor pressure. For safety reasons, the fluid had to have a high flash point and be non-carcinogenic. In the present study we used a commercial solvent called Shell Sol 715 which satisfies most of these requirements (viscosity = 1.09 cp at room temperature, and Bp = 172°C, Fp = 52°C). A copy of the data sheet for this solvent is given in Appendix A.

## 4. EXPERIMENTAL TECHNIQUES

### 4.1 Experimental procedure

A typical test run involved the following steps.

- Cleaning and setting of the reactor system and filling the scrubbing liquid reservoir with 4 liters of clean solvent.

- Start up of the plasma torch and adjustment of its operating conditions, start the circulation of the scrubbing fluid, the powder feed (when using either the silicon vaporizer configurations shown in Figure 9-a or Figure 10) and the methane flow and adjustment of its flow rate.

- At the end of each experiment which typically lasted between 10 to 20 minutes, the reverse procedure was undertaken involving the successive shut down of the methane gas flow, silicon powder feed and of the plasma torch. The scrubbing liquid was kept in circulation to avoid the settling of the powder and to recover the powder deposited on different parts of the reactor/condenser chamber. Fresh solvent was also occasionally added to the system at this stage to complete the recovery of the powder.

- The SiC slurry in the liquid hydrocarbon is next withdrawn from the bottom of the cyclonic separator and the powder recovered using a laboratory centrifuge and dried in a vacuum oven at temperature of 200 to 210°C.

### 4.2 Powder characterization

Special attention was given to powder characterization in order to be able to detect the parametric dependence of the properties of the powders obtained on the operating conditions. The techniques used could be grouped as follows:

- **Chemical techniques**
  The free-carbon content of the powders was determined using thermal gravimetric analysis.

- **Physical techniques**
  These include electron microscopy (SEM and TEM), X-ray diffraction, specific surface area measurements (BET) and the estimation of the average particle size based on the BET measurements.

- **Sintering**
  The evaluation of the sintering properties of the powders was considered outside the scope of the present study and was delayed to the next phase of the investigation.

**Thermal gravimetric** analysis was carried out by slowly heating a 25 mg sample of the powder to 923 K in air and keeping it at this temperature until all of the free carbon present burns and leave the sample as CO, $CO_2$. The estimation of the temperature limit of 923 K, needed to completely oxidize the free-carbon, was established by thermal analysis made on a calibrated mixture of alumina and soot containing 10% soot by weight, and heated to different temperatures (Figure 11). The free-carbon content was calculated from the sample weight loss as follows:

$$w_c = \frac{\text{measured weight loss}}{\text{initial weight of sample}}$$

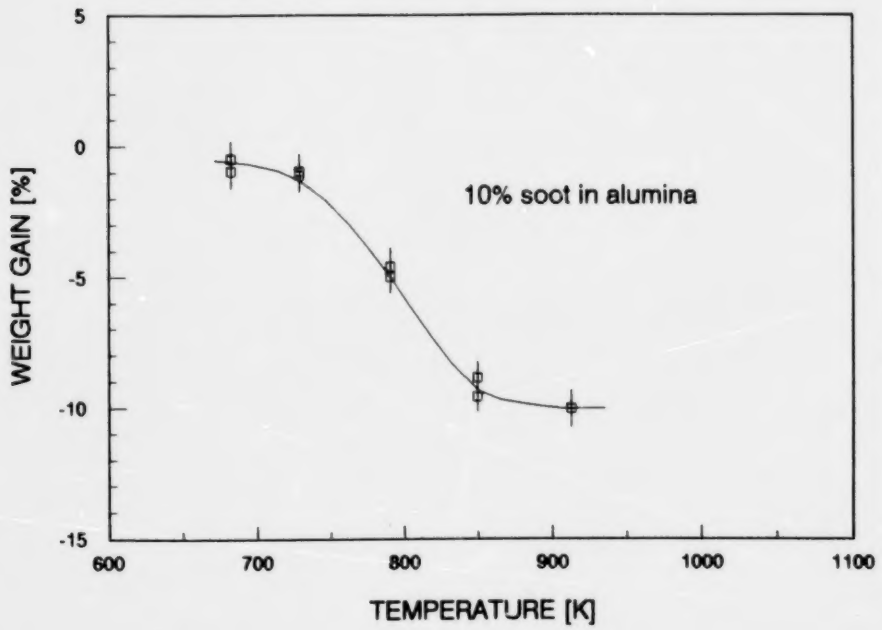


**Figure 11: Weight variation of a mixture 10% soot in alumina powder by thermal gravimetric analysis**

**Scanning Electron Microscopy (SEM)** was used to evaluate the impurities in the powder using EELS (Electron Energy Losses Spectroscopy) for the light elements (O, N, C).

**Transmission Electron Microscopy (TEM)** was used to determine the particle size distribution and the morphology of the crystalline phases of SiC.

Relative weight fraction of crystalline species are determined based on **X-ray diffraction** pattern using the three calibration curves given in Figures 12, 13 and 14. To use theses curves, the surface of the b-SiC peak at 60.0° (that include a-SiC diffraction peak because all b-SiC peaks overlap a-SiC peak), the surface of the a-SiC peak at 38.1° (not shared with the b-SiC), and the Si peak at 28.4°. Each surface is related to the peak intensity and is called respectively $I_{a,b\text{-}SiC}$, $I_{a\text{-}SiC}$ and $I_{Si}$. Calculating the intensity ratio $I_{a\text{-}SiC}/I_{a,b\text{-}SiC}$ and reading on the x axis of Figure 12, gives the mass fraction of a-SiC in the total silicon carbide:

$$W_1 = \frac{w_{a-SiC}}{w_{a-SiC} + w_{b-SiC}}$$

With this value, Figure 13 gives on the y axis the intensity ratio of $I_{a,b\text{-}SiC}$ to that of $I_{pure\ b\text{-}SiC}$ necessary to correct the b-SiC peak at 60.0° as if silicon carbide present was only in the beta form:

$$I_{pure\ b-SiC} = \frac{I_{a,b-SiC}\ \text{measured on the spectrogram}}{\text{y axis value read on Fig. 13}}$$

It is possible now to use the third calibration curve (made with Si and b-SiC standards) by calculating the intensity ratio $I_{Si}/I_{b\text{-}SiC}$ to get the free-silicon concentration among the three crystalline form (x axis of Fig. 14):

$$W_2 = \frac{w_{Si}}{w_{Si} + w_{a-Si} + w_{b-SiC}}$$

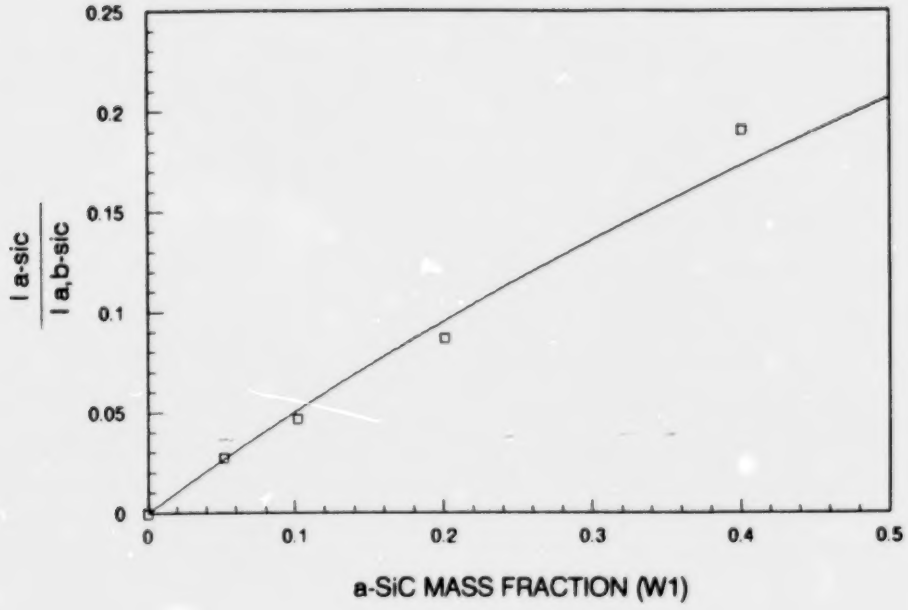


**Figure 12: Diffraction peak intensity ratio of a-SiC at 38.1° and SiC at 60.0° as function of a-SiC content in total SiC**

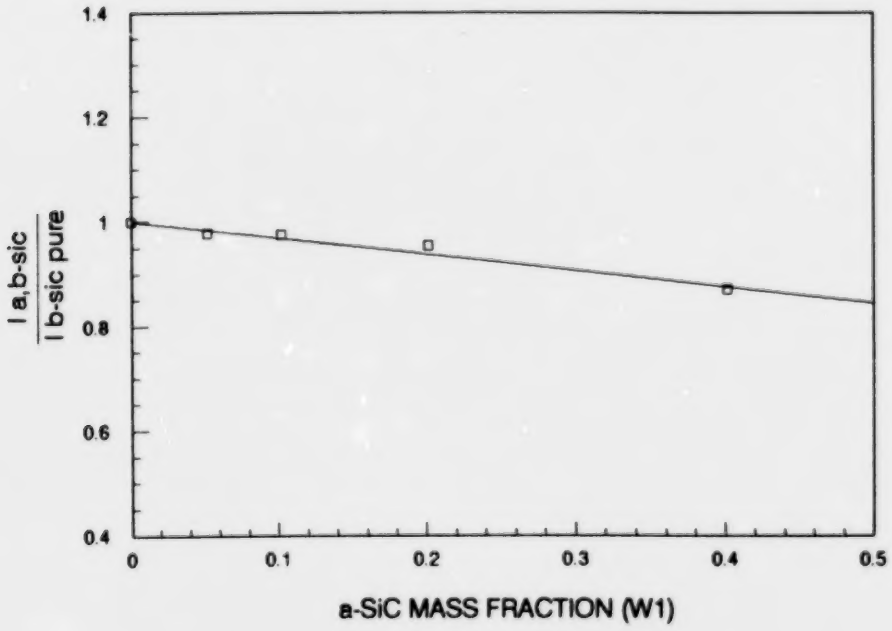


**Figure 13: Diffraction peak intensity ratio of SiC mixture and pure b-SiC at 60.0° as function of a-SiC content in total SiC**

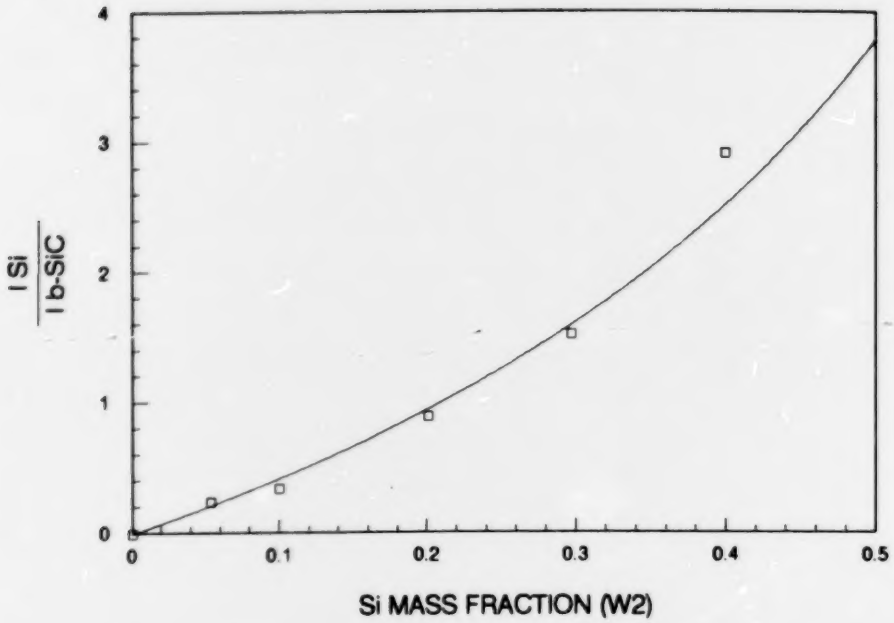


**Figure 14: Diffraction peak intensity ratio of Si at 28.6° and b-SiC at 60.0° as function of Si content in b-SiC**

Knowing the free-carbon content by thermal gravimetric analysis, the respective weight fraction of other species are given by the following matrical system:

$$\begin{pmatrix} 1 & 1 & 1 \\ 0 & w_1 - 1 & w_1 \\ w_2 - 1 & w_2 & w_2 \end{pmatrix} \begin{pmatrix} w_{Si} \\ w_{a\text{-}SiC} \\ w_{b\text{-}SiC} \end{pmatrix} = \begin{pmatrix} 1 - w_c \\ 0 \\ 0 \end{pmatrix}$$

The **specific surface area** of the raw powder are measured using a MICROMERITIC FLOWSORB II 2300 BET specific surface analyzer using nitrogen as adsorbing gas. Mean particle size were estimated from measured specific surface area, $S_s$, assuming equivalent spherical diameter, d:

$$d = \frac{6}{\rho_m S_s}$$

where

$$\frac{1}{\rho_m} = \sum_{i=1}^{n} \frac{w_i}{\rho_i}$$

with $w_i$ and $\rho_i$ the respective weight fraction and pure density of specie i, and n, is the number of species present.

## 5. RESULTS AND DISCUSSION

### 5.1 Silicon powder injection

The first experiments were carried with the direct injection of a silicon powder (-40 μm) in the plasma as illustrated in Figure 9a. A mixture of methane and argon was used as quench gas injected in the tail flame of the plasma jet. The plasma gas was a mixture of argon and hydrogen, and the d.c. torch power was 25 kW. A summary of the operating conditions and the analysis of the powder obtained is given in Tables 1 and 2 respectively, identified as series A.

The powder produced in each of the experiments A09-A15 contained between 55 and 69% w b-SiC with the a-SiC content under 4%. Free-silicon was generally present in the product with a concentration which depends strongly on the C/Si ratio of the feed. For C/Si ratios less than 2.0, free-silicon content is higher than 10% and it surpasses 24% for C/Si ratio near 1.0. The corresponding silicon conversion in the final product was relatively low (~60%). High soot concentrations were observed in a few runs, up to 30% w, of the powder produced.

The specific surface area of these powders was generally over 29 $m^2/g$ with an equivalent spherical diameter of the order of 40 to 70 nm (Table 2).

### 5.2 Silicon sleeve vaporization

The silicon vaporization section used in this case is illustrated in Figure 9b. The operating conditions and the analysis of the powders obtained are given in Tables 1 & 2, C and D Series. Runs C1 and C2 were carried out with the sleeve made of silicon only. Silicon carbide content in the powder produced is above 80% and is mainly in the beta phase. Free-silicon and free-carbon contents of the powder are mostly below 10%.

Because of the lower viscosity of molten silicon and its tendency to drop from the sleeve, 10% w of carbon powder (20% molar) was added to the silicon powder when forming the sleeve. Sleeves made with this modified mixture were used in exp. #D1 and D2 (Tables 1 and 2) which were carried out using nitrogen instead of $Ar/H_2$ as the plasma gas. The plasma power is higher in this case (24.3-26.0 kW) compared to that used in the earlier silicon sleeve experiments (15 kW for C1 & C2). The results show close to 96-98% w silicon conversion to SiC with the produced powder mostly in the b-SiC form, with low free-Si and C contents.

In order to determine the effect of the plasma power level and of the methane feed rate on the silicon conversion, a $2^2$ factorial experimental plan was carried out with a $N_2$ plasma at atmospheric pressure. A summary of the operating conditions and of the analysis of the powders obtained is given in Tables 3 and 4 respectively. It may be noted that even in the absence of methane injection as a quench gas, a certain degree of carburization is achieved 65.7-89.1% w conversion. The source of carbon playing a role in the reaction in this case is the carbon added to the initial mixture (10% w), the sucrose binder used in the formation of the sleeve, and the liquid hydrocarbon scrubbing fluid. The addition of methane as a quench gas results in the increase of the silicon conversion to the 90% range and the appearance of free carbon (3-7% w) in the product. The corresponding free silicon content of the powder is much lower in this case compared to the powders obtained in the absence of methane.

The effect of methane flow rate and of the plasma power on the free carbon and the free silicon content of the powder obtained is show in Figure 15.

Included on this figure is the corresponding variation of the ratio of b-SiC/Total SiC in the product. It may be noted that the plasma power has a relatively small influence on the free-carbon content but results in a major increase of free-silicon in the absence of methane. The effect is obviously due to the increased silicon vaporization rate. It is interesting to note, however, a drop of the b-SiC content of the powder in the presence of $CH_4$ with the increase of the plasma power from 15 to 25 kW. The effect, however, was not statistically as significant as that of the presence of $CH_4$ as shown by the statistical treatment of the data given in Tables 5 and 6.

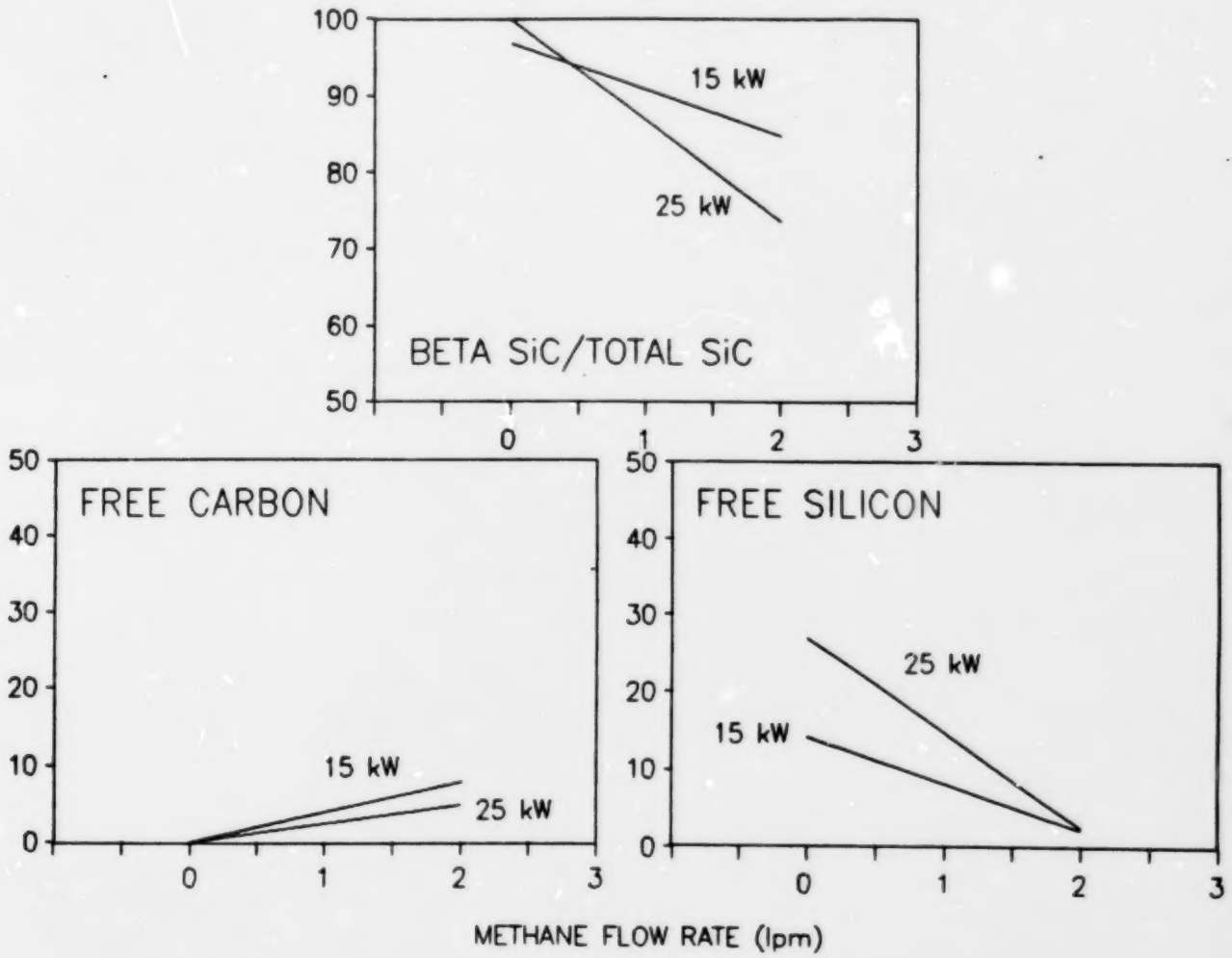


**Figure 15: Trends in product analysis for the $2^2$ factorial plan**

In order to verify for the possible contamination of the SiC-powders with either nitrogen from the plasma gas or oxygen from the atmosphere, detailed examination of the powder obtained in run #E602 was carried out using the EELS (Electron Energy Losses Spectroscopy) at the $CM^2$ Laboratory at Ecole Polytechnique in Montreal. Typical EELS spectrum obtained on a crystalline and an amorphous SiC particle are given in Figures 16 and 17 respectively.

Only the carbon peak can be identified on the EELS spectrum of the crystalline particle (Fig. 16) with neither the nitrogen nor the oxygen peaks detectable indicating the absence of any chemical role of the plasma gas in the synthesis step. The EELS spectrum obtained for the amorphous particle (Fig. 17) shows, on the other hand, a small oxygen peak together with a pronounced carbon peak indicating some contamination from the air, though no nitrogen peaks are detected either. These results seem to confirm that the use of nitrogen as the plasma gas had no detrimental effect on the purity of the powder obtained and justified the continued use of a nitrogen plasma in further work.

While relatively high conversions (76-99% w) were achieved in the last series of experiments, product recovery was relatively low, of the order of 22 to 55%. This was attributed to the loss of the SiC powder and/or SiC/hydrocarbon aerosol with the exhaust gases. Improvement of product recovery in subsequent experiments was achieved through minor modifications of the design and operation of the cyclonic separator and demister units.

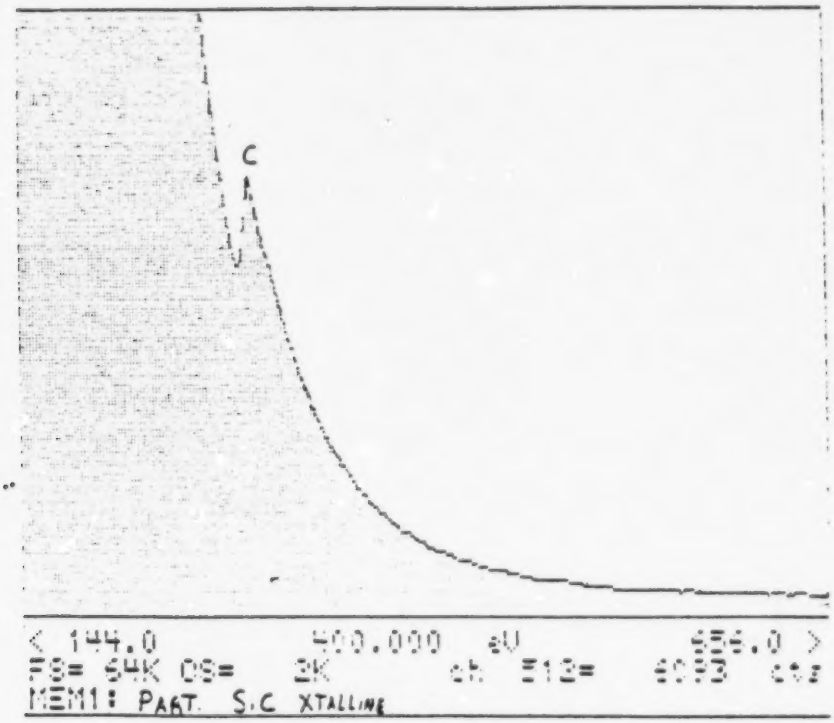


**Figure 16: EELS spectrum of crystalline SiC particles (exp. #E602)**

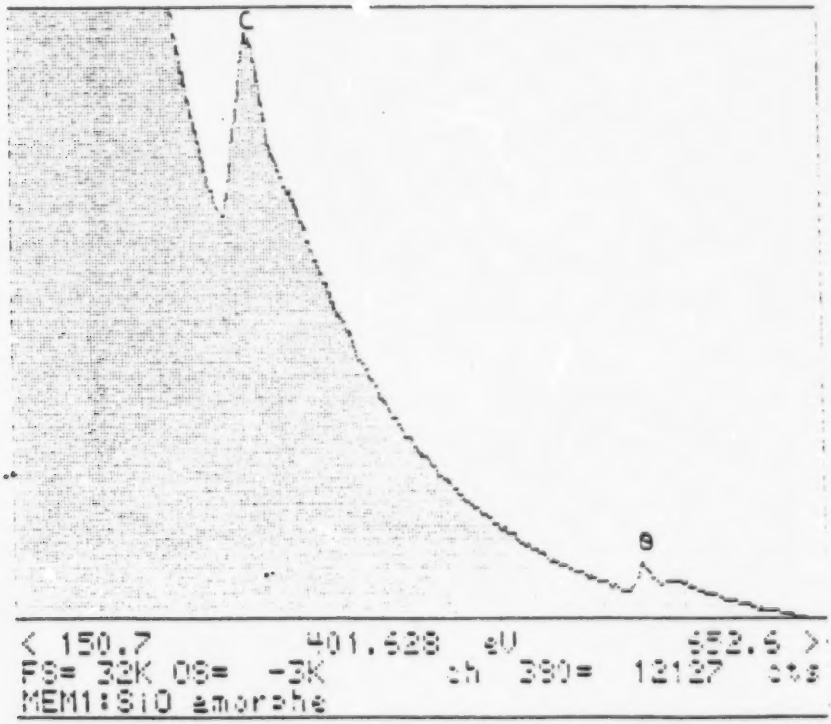


**Figure 17: EELS spectrum of an amorphous particle (exp. #E602)**

Further experiments were carried out according to a short $2^3$ experimental plan in which the methane gas flow rate, the plasma power and the operating pressure were varied as independent parameters. $CH_4$ flow rate was varied in this case between 1.0 and 2.0 l/min compared to the earlier $2^2$ plan in which $CH_4$ flow rate was changed between two OFF/ON levels (0 and 2.0 l/min). A summary of the experimental conditions and of the analysis of the powders obtained is given in Tables 7 and 8 respectively. The results are presented graphically in Figure 18 and a complete statistical analysis of the data is given in Tables 9 and 10.

The results show a significant influence of the operating pressure on the free carbon and free-silicon content of the product with the atmospheric pressure operation favoring the reduction of the free-silicon content of the powder. While the pressure did not seem to have an influence on the (b-SiC/Total SiC) ratio in the product, the plasma power showed a moderate influence. The high power operation favored in this case an increase of the (b-SiC/Total SiC) ratio, which seems contradictory to our earlier results obtained in the $2^2$ plan.

It may be noted from Tables 8 and 9 that, depending on the operating conditions, the free-carbon content of the product could be controlled below 4% w, free-silicon below 2% w, with over 93% w of the total SiC obtained in the b-SiC form. In the case of run #104 for example, the overall silicon conversion was above 98% w with close to 50% w product recovery. The specific surface area of the powder obtained was 49.4 $m^2/g$ with a corresponding mean particle diameter of 39 nm. Transmission Electron Micrographs of the powders obtained in exp. #112 are shown in Figure 19 where the typical trigonal and hexagonal shapes of the ultrafine particles can be seen.

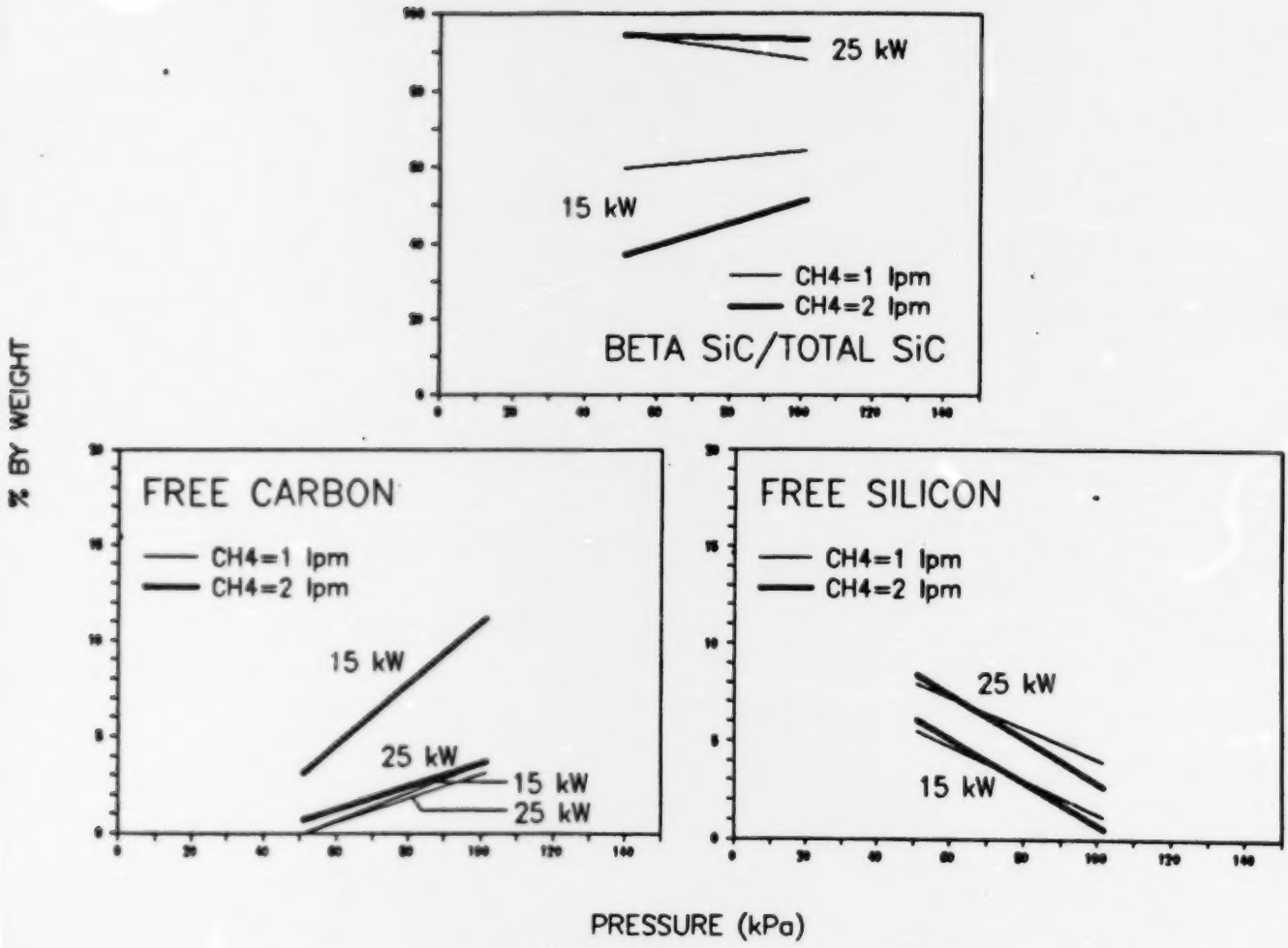


**Figure 18: Trends in product analysis for the $2^3$ factorial plan**

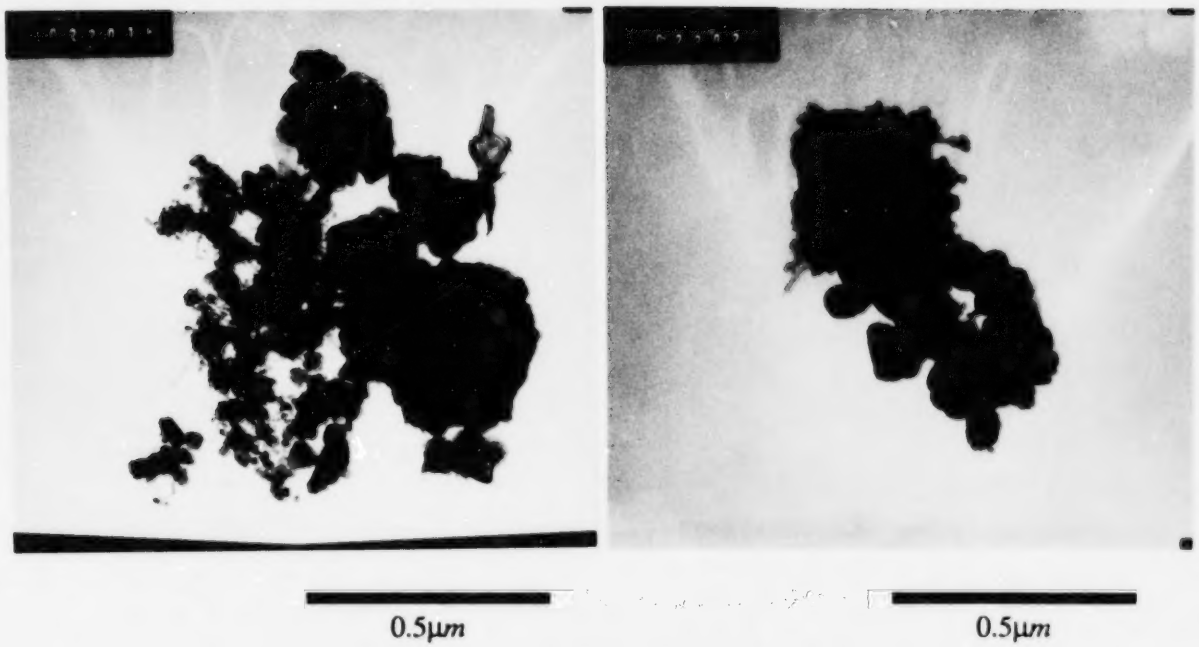


**a) Run 103, Plasma: N2, 25.5 kW, Pressure: 101.7 kPa.**

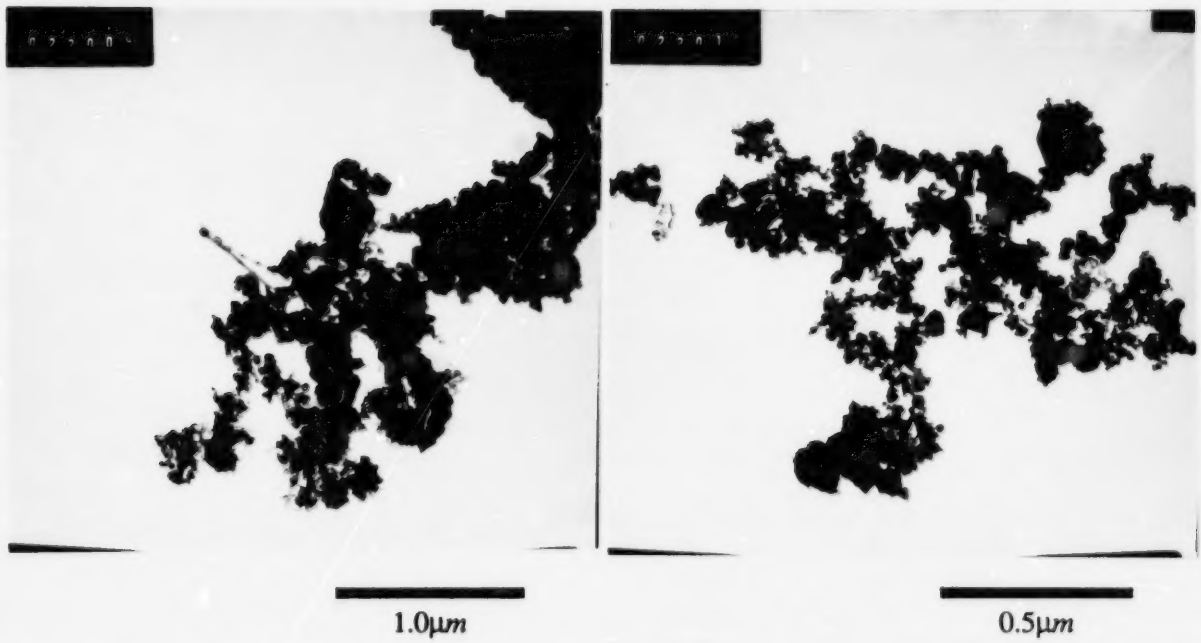


**b) Run 112, Plasma: N2, 25.8 kW, Pressure: 50.9 kPa.**

**Figure 19: Typical micrographs of SiC particles.**

### 5.3 CSC reactor

Eleven runs were performed using the continuous silicon carburization (CSC) reactor illustrated in Figure 10, with different carbon to silicon atomic ratios in the feed. The plasma gas was a mixture of $Ar/N_2$, the plasma power was fixed at 25 kW and the pressure was kept at 101.7 kPa. A summary of the results and of the product analysis is given in Tables 11 and 12 respectively.

The expected liquid silicon bath did not occur, however, in the graphite crucible. Instead, carburization of the injected silicon powder seems to take place in-flight with the entrainment of relatively large particles of Si and SiC with the exhaust gases out of the reactor. This gave rise to relatively high free-silicon content of the powder (more than 8% w). The free-carbon content of the powder was also relatively high (of the order of 5-7% w). Because of the deposition of the powder on the different sections of the graphite reactor from which they could not be easily recovered, no meaningful product recovery data could be obtained for these runs.

In spite of the relatively high conversions obtained with this CSC reactor (above 90% w), the low product recovery and the numerous operating problems led us to the conclusion that for the next phase of the investigation we might have to go back to the sleeve design or modifications of it using for example a rotating vertical reactor. In either case it will be necessary to achieve a continuous mode of operation without sacrificing conversion, energy efficiency or product recovery.

**Table 1: Conditions used for the Preliminary tests.**

| | plasma | | | | feed | | |
|---|---|---|---|---|---|---|---|
| # exp | plasma gas (vol. %) | | | plasma power | $\dot{m}$silicon | $CH_4$ flowrate | C/Si |
| | Ar | $H_2$ | $N_2$ | (kW) | (g/min) | (lpm) | (molar) |
| A09 | 50 | 50 | -- | 24.5 | 4.4 | 7.8 | 2.0 |
| A10 | 50 | 50 | -- | 27.5 | 5.3 | 7.8 | 1.7 |
| A12 | 50 | 50 | -- | 25.5 | 2.0 | 7.8 | 4.5 |
| A13 | 50 | 50 | -- | 25.5 | 4.5 | 9.0 | 2.3 |
| A14 | 50 | 50 | -- | 27.0 | 6.6 | 5.0 | 0.9 |
| A15 | 50 | 50 | -- | 24.7 | 9.0 | 9.0 | 1.1 |
| C1* | -- | -- | 100 | 18.9 | 3.8 | 10.0 | 3.6 |
| C2* | 60 | 40 | -- | 10.2 | 3.6 | 10.0 | 3.6 |
| D1* | -- | -- | 100 | 24.3 | 6.0 | 4.0 | 1.1 |
| D2* | -- | -- | 100 | 26.0 | 8.1 | 2.0 | 0.6 |

total $V_{plasma}$ = 47.2 lpm except * V = 23.6 lpm

**Table 2: Analysis of the SiC powders from Preliminary tests.**

| | Powder compositions (weight %) | | | | spec. surface | particle diameter | conv. |
|---|---|---|---|---|---|---|---|
| # exp | C | Si | α-SiC | β-SiC | ($m^2$/g) | (nm) | (%) |
| A09 | 14.5 | 13.3 | 2.7 | 69.5 | 29.6 | 73 | 78.7 |
| A10 | 30.8 | 10.4 | 2.5 | 56.4 | 30.3 | 77 | 79.9 |
| A12 | 26.7 | 7.4 | 3.8 | 62.1 | 35.7 | 63 | 86.2 |
| A13 | 27.2 | 6.0 | 1.8 | 64.9 | 44.7 | 51 | 88.6 |
| A14 | 11.3 | 24.9 | n.d. | 63.8 | 39.3 | 56 | 64.2 |
| A15 | 19.8 | 24.4 | n.d. | 55.9 | 38.3 | 60 | 61.6 |
| C1 | 4.4 | 3.3 | 17.6 | 74.6 | 59.0 | 33 | 95.1 |
| C2 | 8.0 | 9.6 | n.d. | 82.4 | 90.9 | 22 | 85.7 |
| D3 | 8.0 | 1.4 | 5.4 | 85.2 | 29.4 | 67 | 97.8 |
| D4 | 0.8 | 2.8 | 6.4 | 90.0 | 59.3 | 32 | 96.0 |

n.d. = not detected
A: Si powder injection
C: 10% sucrose-silicon sleeve
D: 15% sucrose-carbon-silicon sleeve

**Table 3: Conditions for the $2^2$ factorial experiments.**
**(silicon sleeve vaporization)**

| # exp | plasma gas | plasma power (kW) | pressure (kPa) | CH4 flowrate (lpm) | mass of block evap. (g) | test duration (min) | mass of powder produced (g) |
|---|---|---|---|---|---|---|---|
| E801 | $N_2$ | 15.7 | 101.7 | 0 | 14.39 | 3.0 | 3.34 |
| E501 | $N_2$ | 15.9 | 101.7 | 0 | 15.36 | 5.0 | 4.14 |
| E701 | $N_2$ | 15.9 | 101.7 | 0 | 15.50 | 7.0 | 5.02 |
| E504 | $N_2$ | 15.9 | 101.7 | 2 | 15.57 | 5.0 | 10.50 |
| E505 | $N_2$ | 25.1 | 101.7 | 0 | 20.23 | 5.0 | 7.76 |
| E602 | $N_2$ | 25.7 | 101.7 | 2 | 17.13 | 3.0 | 6.27 |
| E302 | $N_2$ | 25.3 | 101.7 | 2 | 18.65 | 5.0 | 7.41 |
| E402 | $N_2$ | 25.2 | 101.7 | 2 | 18.30 | 7.0 | 8.79 |

**Table 4: Analysis of the SiC powders from the $2^2$ factorial experiments.**
**(silicon sleeve vaporization)**

| | Powder compositions (weight %) | | | | | spec. surf. | particle diameter | recov | conv. |
|---|---|---|---|---|---|---|---|---|---|
| #exp | C | Si | α-SiC | β-SiC | $\frac{\beta-SiC}{SiC}$ | ($m^2/g$) | (nm) | (%) | (%) |
| E801 | n.d. | 16.1 | 5.2 | 78.7 | 93.8 | 82.9 | 24 | 21.7 | 79.0 |
| E501 | n.d. | 7.9 | n.d. | 92.1 | 100.0 | 76.6 | 25 | 24.4 | 89.1 |
| E701 | n.d. | 18.4 | n.d. | 81.6 | 100.0 | 67.8 | 29 | 30.6 | 75.6 |
| E504 | 7.8 | 2.3 | 14.2 | 75.8 | 84.2 | 79.8 | 25 | 55.0 | 96.5 |
| E505 | n.d. | 26.8 | n.d. | 73.2 | 100.0 | 50.1 | 41 | 37.4 | 65.7 |
| E602 | 6.0 | 1.8 | 24.1 | 68.2 | 73.9 | 70.4 | 28 | 30.4 | 97.3 |
| E302 | 3.4 | 1.0 | 20.0 | 75.5 | 79.1 | 54.3 | 35 | 33.7 | 98.5 |
| E402 | 5.4 | 5.1 | 29.5 | 60.0 | 67.0 | 63.9 | 31 | 40.7 | 92.5 |

n.d. = not detected

**Table 5: Low and high level for the $2^2$ factorial analysis. (silicon sleeve vaporization)**

| parameter | low level<br>- | high level<br>+ |
|---|---|---|
| A: plasma power (kW)<br>B: $CH_4$ flow rate (lpm) | 15<br>0 | 25<br>2 |

**Table 6: Statistical treatment of the data for the $2^2$ factorial plan.**

FREE CARBON

| Effect | Sum of square | degree of freedom | Mean of square | $F_0$ |
|---|---|---|---|---|
| A: plasma power (kW) | 6.3 | 1 | 6.3 | 6.3 |
| B: $CH_4$ flowrate(lpm) | 121.0 | 1 | 121.0 | **121.0*** |
| interaction A+B | 6.3 | 1 | 6.3 | 6.3 |
| error | 4.0 | 4 | 1.0 | |
| total | 137.6 | 7 | | |

FREE SILICON

| Effect | Sum of square | degree of freedom | Mean of square | $F_0$ |
|---|---|---|---|---|
| A: plasma power (kW) | 126.8 | 1 | 126.8 | 7.3 |
| B: $CH_4$ flowrate(lpm) | 972.0 | 1 | 972.0 | **56.2*** |
| interaction A+B | 115.3 | 1 | 115.3 | 6.7 |
| error | 69.15 | 4 | 17.3 | |
| total | 1283.2 | 7 | | |

β-SiC CONTENT IN TOTAL SILICON CARBIDE

| Effect | Sum of square | degree of freedom | Mean of square | $F_0$ |
|---|---|---|---|---|
| A: plasma power (kW) | 58.1 | 1 | 58.1 | 2.3 |
| B: $CH_4$ flowrate(lpm) | 1224.1 | 1 | 1224.1 | **48.1*** |
| interaction A+B | 122.9 | 1 | 122.9 | 4.8 |
| error | 101.9 | 4 | 25.47 | |
| total | 1507.0 | 7 | | |

**F(.25;1;4)=7.71; *significant at 95%**

**Table 7: Conditions used for the $2^3$ factorial experiments. (Silicon sleeve vaporization)**

| # exp | plasma gas | plasma power (kW) | pressure (kPa) | CH4 flowrate (lpm) | mass of block evap. (g) | test duration (min) | mass of powder produced (g) |
|---|---|---|---|---|---|---|---|
| 101 | $N_2$ | 15.3 | 101.7 | 1.0 | 6.88 | 5.0 | 3.86 |
| 102 | $N_2$ | 15.9 | 101.7 | 2.0 | 4.79 | 5.0 | 3.30 |
| 103 | $N_2$ | 25.7 | 101.7 | 1.0 | 18.11 | 5.0 | 9.97 |
| 203 | $N_2$ | 25.5 | 101.7 | 1.0 | 18.46 | 5.0 | 6.95 |
| 303 | $N_2$ | 25.7 | 101.7 | 1.0 | 15.24 | 5.0 | 7.02 |
| 104 | $N_2$ | 25.4 | 101.7 | 2.0 | 18.50 | 5.0 | 10.17 |
| 109 | $N_2$ | 15.5 | 50.9 | 1.0 | 8.00 | 5.0 | 5.57 |
| 110 | $N_2$ | 15.1 | 50.9 | 2.0 | 7.99 | 5.0 | 4.52 |
| 111 | $N_2$ | 25.3 | 50.9 | 1.0 | 17.20 | 5.0 | 10.14 |
| 112 | $N_2$ | 25.8 | 50.9 | 2.0 | 18.51 | 5.0 | 12.82 |

**Table 8: Analysis of the SiC powders from the $2^3$ factorial experiments. (Silicon sleeve vaporization)**

| | Powder compositions (weight %) | | | | | spec. surf. | particle diameter | recov | conv. |
|---|---|---|---|---|---|---|---|---|---|
| #exp | C | Si | α-SiC | β-SiC | $\frac{\beta-SiC}{SiC}$ | ($m^2/g$) | (nm) | (%) | (%) |
| 101 | 3.6 | 2.7 | 33.6 | 60.1 | 64.1 | 78.6 | 25 | 47.9 | 96.0 |
| 102 | 11.2 | 0.5 | 42.7 | 45.5 | 51.6 | 82.6 | 26 | 53.6 | 99.2 |
| 103 | 3.3 | 0.9 | 5.2 | 90.6 | 94.6 | 35.8 | 54 | 46.8 | 98.7 |
| 203 | 2.4 | 9.0 | 13.3 | 75.3 | 85.0 | 47.1 | 42 | 33.4 | 87.3 |
| 303 | 3.5 | 1.7 | 14.8 | 80.0 | 84.4 | 62.3 | 31 | 39.2 | 97.5 |
| 104 | 3.7 | 1.1 | 6.4 | 88.8 | 93.3 | 49.4 | 39 | 47.6 | 98.4 |
| 109 | n.d. | 8.4 | 36.8 | 54.8 | 59.8 | 68.1 | 28 | 63.1 | 88.4 |
| 110 | 3.1 | 6.1 | 57.0 | 33.8 | 37.2 | 98.6 | 20 | 49.3 | 91.2 |
| 111 | n.d. | 7.9 | 5.1 | 86.9 | 94.5 | 32.7 | 59 | 53.3 | 89.1 |
| 112 | 0.7 | 5.5 | 5.0 | 88.8 | 94.6 | 29.1 | 66 | 61.6 | 92.3 |

n.d. = not detected

**Table 9: Low and high level for the $2^3$ factorial plan. (Silicon sleeve vaporization)**

| parameter | low level - | high level + |
|---|---|---|
| A: $CH_4$ flow rate (lpm) | 1 | 2 |
| B: pressure (kPa) | 50.9 | 101.7 |
| C: plasma power (kW) | 15 | 25 |

**Table 10: Statistical analysis of the data for the $2^3$ factorial plan.**

FREE CARBON

| Effect | Sum of square | degree of freedom | Mean of square | $F_0$ |
|---|---|---|---|---|
| $CH_4$ flow rate(lpm) | 18.0 | 1 | 18.0 | 3.6 |
| Pressure (kPa) | 39.6 | 1 | 39.6 | **7.9*** |
| Plasma power (kW) | 13.5 | 1 | 13.5 | 2.7 |
| error | 20.1 | 4 | 5.03 | |
| total | 91.2 | 7 | | |

FREE SILICON

| Effect | Sum of square | degree of freedom | Mean of square | $F_0$ |
|---|---|---|---|---|
| $CH_4$ flow rate(lpm) | 11.8 | 1 | 11.8 | **36.3*** |
| Pressure (kPa) | 48.5 | 1 | 48.5 | **149.2*** |
| Plasma power (kW) | 0.1 | 1 | 0.1 | 0.3 |
| error | 1.3 | 4 | 0.33 | |
| total | 61.5 | 7 | | |

β-SiC CONTENT IN TOTAL SILICON CARBIDE

| Effect | Sum of square | degree of freedom | Mean of square | $F_0$ |
|---|---|---|---|---|
| $CH_4$ flow rate(lpm) | 110.3 | 1 | 110.3 | 1.4 |
| Pressure (kPa) | 14.9 | 1 | 14.9 | 0.2 |
| Plasma power (kW) | 3108.7 | 1 | 3108.7 | **38.2*** |
| error | 325.0 | 4 | 81.3 | |
| total | 3558.9 | 7 | | |

F(0.25;1;4)=7.71; *significant at 95%

**Table 11: Conditions used for the CSC Reactor experiments.**

| # exp | plasma gas (%vol) | | plasma power | pressure | $CH_4$ flowrate | $\dot{m}$ silicon | feeding time | mass of powder produced |
|---|---|---|---|---|---|---|---|---|
| | Ar | $N_2$ | (kW) | (kPa) | (lpm) | (g/min) | (min) | (g) |
| F1 | 40 | 60 | 25.9 | 101.7 | 4.6 | 1.6 | 7 | 7.16 |
| F2 | 40 | 60 | 24.4 | 101.7 | 3.9 | 3.1 | 15 | 25.9 |
| F3 | 40 | 60 | 24.5 | 101.7 | 3.3 | 3.0 | 14 | 22.3 |
| F4 | 40 | 60 | 24.5 | 101.7 | 4.7 | 3.4 | 13 | 28.3 |
| F5 | 40 | 60 | 25.1 | 101.7 | 2.9 | 3.1 | 15 | 20.6 |
| F6 | 40 | 60 | 25.5 | 101.7 | 3.6 | 3.0 | 13 | 33.8 |
| F7 | 50 | 50 | 26.4 | 101.7 | 2.9 | 2.7 | 9 | 18.8 |
| F8 | 50 | 50 | 25.9 | 101.7 | 3.1 | 2.8 | 13 | 24.3 |
| F9 | 50 | 50 | 25.5 | 101.7 | 3.0 | 2.2 | 8 | 16.8 |
| F10 | 50 | 50 | 25.9 | 101.7 | 3.4 | 2.3 | 11 | 28.2 |
| F11 | 50 | 50 | 25.2 | 101.7 | 2.7 | 2.5 | 9 | 16.2 |

**Table 12: Analysis of the SiC powders**

| | Powder compositions (weight %) | | | | | spec. surf. | particle diameter | recov | conv. |
|---|---|---|---|---|---|---|---|---|---|
| #exp | C | Si | α-SiC | β-SiC | $\frac{\beta-SiC}{SiC}$ | ($m^2/g$) | (nm) | (%) | (%) |
| F1 | 20.6 | 4.0 | 3.1 | 72.3 | 95.9 | 53.8 | 39 | 36.0 | 93.0 |
| F2 | 3.5 | 3.1 | 3.5 | 90.0 | 96.3 | 30.9 | 63 | 38.8 | 95.5 |
| F3 | 1.2 | 4.0 | tr | 94.8 | >99. | 20.8 | 92 | 37.1 | 94.3 |
| F4 | 5.1 | 4.1 | 7.2 | 83.6 | 92.1 | 30.9 | 63 | 43.6 | 93.4 |
| F5 | 6.1 | 0.8 | 8.3 | 84.7 | 91.1 | -- | -- | 29.1 | 98.8 |
| F6 | 0.7 | 1.4 | 3.1 | 94.7 | 96.8 | 17.5 | 108 | 60.5 | 98.0 |
| F7 | 0.5 | 12.5 | 5.6 | 81.3 | 93.6 | 27.7 | 71 | 55.8 | 83.0 |
| F8 | 5.2 | 5.2 | 4.2 | 85.4 | 95.3 | 24.7 | 80 | 44.6 | 92.3 |
| F9 | 4.4 | 7.1 | 1.3 | 87.2 | 98.5 | 16.8 | 117 | 92.3 | 89.7 |
| F10 | 4.6 | 4.9 | 2.8 | 87.8 | 96.9 | 34.1 | 57 | 76.2 | 92.8 |
| F11 | 3.8 | 6.7 | 1.3 | 88.2 | 98.5 | 31.3 | 63 | 86.5 | 90.3 |

# APPENDIX A: DATA SHEET FOR SHELL SOL 715

**Code Shell**
**648-500**

# Shell Sol* 715

Shell Sol 715 est un solvant isoparaffinique synthétisé à partir d'hydrocarbures spécifiques et dans des conditions qui excluent pratiquement toute formation de fractions odorantes. Il en résulte un produit extrêmement stable qui, dans des conditions normales d'emploi et d'entreposage prolongé, demeure presque totalement inodore.

**Usages:**
enduits, aérosols, produits spéciaux, support de réactions.

| **Caractéristiques** | | **Méthode d'ess** |
|---|---|---|
| Densité à 15 °C, kg/L | 0,757 | D 129 |
| Point d'éclair, vase clos Tag, °C | 52,0 | D 5 |
| Point d'aniline, °C | 85,6 | D 61 |
| Indice kauri-butanol | 26,0 | D 113 |
| **Composition,** % en volume | | D 278 |
| hydrocarbures paraffiniques | 100 | |
| hydrocarbures naphténiques | 0 | |
| hydrocarbures aromatiques | 0 | |
| **Temps d'évaporation,** secondes à 25 °C | | D 353 |
| 10% de produit évaporé | 390 | |
| 20% | 780 | |
| 30% | 1200 | Évaporimètr |
| 40% | 1680 | automatique She |
| 50% | 2160 | à pellicule minc |
| 60% | 2760 | |
| 70% | 3360 | |
| 80% | 4080 | |
| 90% | 4980 | |
| 95% | 5580 | |
| 100% | 6840 | |
| **Intervalle de distillation,** °C | | D 8 |
| point initial de distillation | 179,0 | |
| 10% de produit recueilli | 180,0 | |
| 30% | 182,0 | |
| 50% | 183,5 | |
| 70% | 186,5 | |
| 90% | 195,0 | |
| point final | 203,0 | |

*Marque déposée — Shell Canada Limitée

*Le contenu de cette publication est exact, au meilleur de nos connaissances, au moment de l'impression. Les renseignements qui y sont donnés peuvent cependant être modifiés sans préavis et devraient par conséquent être vérifiés avant utilisation des produits.*

*Les recommandations relatives aux usages ou applications des produits ne s'accompagnent d'aucune garantie, car les conditions dans lesquelles ils seront employés échappent au contrôle de Shell. Rien de ce qui est contenu dans la présente publication ne devrait être interprété comme une recommandation d'utiliser un produit contrairement aux exigences de brevets existants.*

**Propriétés générales de Shell Sol 715**

| Caractéristiques | | Méthodes d'essai |
|---|---|---|
| Taux relatif d'évaporation de 90 % de Shell Sol 715 (par rapport à l'acétate de butyle normal = 1,0) | <0,1 | D 3539 |
| Corrosion à la lame de cuivre, au point d'ébullition | n° 1 | D 130 |
| Essai au plombite de soude | négatif | D 484 |
| Couleur Saybolt | +30 | D 156 |
| Indice de réfraction, n 20/D | 1,4234 | D1218 |
| Poids moléculaire moyen | 152 | |
| Degré de polarisation | 0 | |
| Liaison hydrogène | pas de liaison | |
| Paramètre de solubilité | 7,4 | |
| Odeur (avec échantillon ordinaire) | non décelable | |